Mineralium Deposita (2003) 38: 356–369
DOI 10.1007/s00126-002-0312-5

ARTICLE

Sonja L. Boorman · James B. McGuire
Alan E. Boudreau · F. Johann Kruger

Fluid overpressure in layered intrusions: formation of a breccia pipe in the Eastern Bushveld Complex, Republic of South Africa

Received: 16 February 2001 / Accepted: 26 June 2002 / Published online: 6 September 2002

Abstract Fluids and volatile fluid overpressures in layered intrusions are becoming recognized as having important functions in magma chamber processes for the formation of magmatic structures and for the movement and concentration of economically important ore elements. We re-examine a breccia pipe in the Bushveld Complex to investigate the role of volatile fluid overpressure in its emplacement. This 10-m-diameter breccia pipe was emplaced vertically in the anorthosite of the Upper Critical Zone of the Bushveld Complex and contains blocks of Bushveld anorthosite, norite, and pyroxenite, apparently derived from lower in the stratigraphy. The blocks are commonly elongate, and are tightly packed within an ultramafic pegmatite groundmass. Ultramafic pegmatitic dikes radiate bilaterally from the pipe. Microprobe analyses of plagioclase in the breccia pipe blocks reveal that these grains are unzoned and have higher anorthosite content ($\sim An_{85}$) than host rock plagioclase ($\sim An_{75}$), indicating that the breccia pipe blocks were transported considerable vertical distances. Whole-rock major- and trace-element data show enrichment in fluid-soluble incompatible elements, supporting the role of volatile fluids in the formation of the pipe. A model is examined in which the segregation of a fluid phase from interstitial liquids in the cumulate section below the breccia pipe leads to the development of sufficient overpressure for its explosive emplacement. Fluid overpressure can develop by compaction and during crystallization of plagioclase-saturated silicate liquids as fluids exsolve from the solidifying interstitial liquid. If fluids separate faster than they can escape from the crystal pile, significant overpressures can develop. The minimum fluidization velocity which would be required to emplace blocks of the size and density found within the breccia pipe is found to be 10–110 m/s. The crystallization model predicts the development of about 400 bar of overpressure, an amount calculated to be sufficient for pipe emplacement.

Keywords Bushveld Complex · Breccia pipe · Fluidization · Overpressure

Editorial handling: O. Thalhammer

S.L. Boorman (✉) · A.E. Boudreau
Division of Earth and Ocean Sciences,
Duke University, Durham NC, 27708, USA
E-mail: sonja.boorman@duke.edu
Tel.: +1-919-6819339
Fax: +1-919-6845833

J.B. McGuire
Department of Geological Sciences,
University of Texas, Austin, TX, USA

F.J. Kruger
Hugh Allssopp Laboratory,
University of the Witwatersrand, Wits 2050, RSA

Introduction

Eugen Stumpfl, whose work this special volume honors, was one of the first to recognize the evidence for and potential importance of fluids in platinum-group element (PGE) ore petrogenesis in layered intrusions (e.g., Stumpfl and Tarkian 1976; Stumpfl and Rucklidge 1982). Recent work continues to expand on the role of fluids and fluid overpressure in mafic magma chambers in general (e.g., Tait and Jaupert 1992) and in layered intrusions in particular (e.g., Stumpfl and Rucklidge 1982; Ballhaus and Stumpfl 1985; Boudreau 1992). The presence of either fluid phases or volatile-rich silicate liquids in layered intrusions is evidenced by hydrous minerals, graphite and pegmatoidal textures. Mobilization of such fluids has been implicated in the formation of ultramafic pegmatites in the Bushveld and other layered complexes (e.g., Viljoen and Scoon 1985; McBirney and Sonnenthal 1990; McBirney and Naslund 1990; Mogessie et al. 1991; Scoon and Mitchell 1994).

In the Bushveld Complex, such pegmatoidal horizons are the subject of great interest as they are often host to economic PGE deposits. Scoon and Mitchell (1994) proposed that transgressive ultramafic bodies form from

the immiscible separation of an iron-rich liquid from its felsic counterpart, such that the denser, iron-rich liquid drains downwards to form transgressive pegmatitic bodies. It has alternatively been suggested that these ultramafic pegmatitic rocks are channel ways for upward fluid migration through the crystal pile whereby hydration from foot-wall cumulates leads to isothermal melting and the formation of a melt-rich horizon (Nicholson and Mathez 1991).

Additional evidence for fluid mobilization in layered intrusions is found in mineral chemistry and rock structures. High-Cl apatites found in the rocks beneath the Merensky reef have been interpreted as indicating Cl enrichment from upwardly migrating fluids (Boudreau et al. 1986; Boudreau and Kruger 1990; cf. Boudreau and McCallum 1989), and pothole structures in the Bushveld Complex have been modeled as resulting from fluid overpressure (Boudreau 1992). Such potholes are often associated with discordant pegmatitic bodies comprised of hydrous minerals and which are interpreted to have been fluid escape channels (Ballhaus and Stumpfl 1985; Buntin et al. 1985). The limited published data available indicate that rocks from pothole structures are enriched in elements which are mobile in aqueous fluids, relative to immobile incompatible elements (e.g., Ballhaus 1988). The degassing of such fluids from an interstitial melt in a crystallizing pile can lead to overpressure development (Boudreau 1992).

Ferguson and McCarthy (1970) were the first to describe this breccia pipe which is wholly within the Bushveld Complex, and also suggested it formed in response to fluid overpressure. We expand on the study of Ferguson and McCarthy and examine the physical characteristics of the breccia pipe and its relation to the surrounding country rock, based on whole-rock and major- and trace-element analyses of the blocks within the pipe and country rocks as well as microprobe analyses of the constituent minerals. The data and field evidence show that the blocks in the pipe are not in situ but were transported from below. Furthermore, we establish that fluid overpressure generated by crystallization of fluid-saturated interstitial silicate liquid can give rise to the overpressures required for the explosive emplacement of the breccia pipe.

Geology of the Bushveld Complex

The Bushveld Complex is a layered mafic intrusion with an aerial extent of approximately 66,000 km^2 situated in the Kaapvaal province of the Republic of South Africa (Fig. 1). The Bushveld Complex is a member of the Bushveld magmatic province which comprises three different magmatic events, starting with the eruption of the Rooiberg felsites approximately 2.06 Ga ago (Walraven 1988). The Rooiberg felsites form the roof to the economically important, layered mafic rocks which comprise the Bushveld Complex proper, which was intruded beneath the felsites during multiple magmatic pulses. Three to four distinct magmatic pulses have been proposed, based on Sr isotope distinctions at the Critical Zone/Main Zone boundary and at the Main Zone/Upper Zone boundary (Kruger and Marsh 1982; Kruger et al. 1986). Finally, the Bushveld granite was intruded

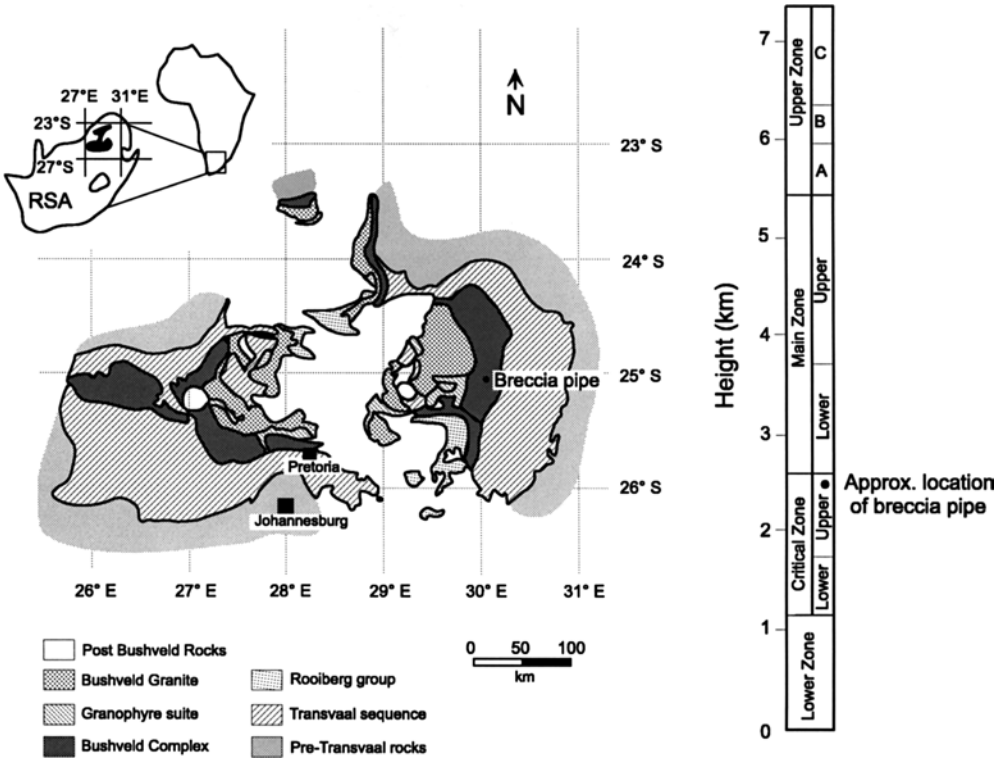

Fig. 1 General location map and stratigraphic section for the Bushveld Complex showing the breccia pipe location (Willmore et al. 2000)

into the center of the complex at 2.04 Ga (Walraven 1988). Although these three members of the Bushveld igneous suite are spatially and temporally related, their genetic relationships are unknown.

The layered rocks of the Bushveld Complex form a lopolithic intrusion which is 7–9 km thick. The stratigraphic divisions of the Bushveld Complex are described in detail by Eales and Cawthorn (1996). The stratigraphy of the Bushveld is, from the bottom up: (1) the Lower Zone, (2) the Critical Zone, (3) the Main Zone, and (4) the Upper Zone (Fig. 1). The Lower Zone is 800–1,000 m thick and consists primarily of layers of pyroxenite, dunite, and harzburgite with some chromite with small amounts of intercumulus plagioclase, biotite, and clinopyroxene. The boundary between the Lower Zone and the Critical Zone occurs where the modal abundance of interstitial plagioclase increases to roughly 4%. The Critical Zone is split into the Upper Critical and Lower Critical zones, with the boundary between the two occurring where plagioclase appears as an euhedral (cumulus) phase. The boundary between the Critical Zone and the Main Zone is usually taken to be the base of the Merensky reef, and that of the Upper Zone the pyroxenite marker, following the suggestion of Kruger (1994).

Geology of the breccia pipe

The studied breccia pipe crosscuts the rhythmically layered, mottled anorthosite of the Upper Critical Zone of the Bushveld Complex (Ferguson and McCarthy 1970), about 2.4 km above the base of the complex (Fig. 1). The pipe is exposed in cross section along a gully wall formed by a small stream (Fig. 2). The body is roughly circular in map view and has a diameter of about 10 m. The contact between the pipe and wall rock is generally very well preserved, and is at a high angle to regional layering.

Sub-angular to subrounded blocks of Bushveld lithologies are fit tightly together in the body of the pipe (Fig. 3a). The blocks are comprised primarily of norites and anorthosites, with lesser amounts of pyroxenite (Fig. 3b). The blocks in the pipe are up to about 15 cm in diameter but range up to 1 m in length. Blocks with high aspect ratios tend to have their long axis vertically oriented (Fig. 3c). The larger blocks are concentrated in the center of the pipe, and there is a gradation to the eastern side with the smallest blocks along the eastern contact (Fig. 3d). All of the material in the pipe comprises Bushveld lithologies. In addition to the transported blocks, fragments of the local anorthositic host rock have been entrained in the pipe. These fragments are angular and occur near the periphery of the pipe (Fig. 3e), and appear to have been ripped from the wall and entrained in the breccia pipe.

A pegmatite fills much of the interstitial areas of the pipe and occurs as veinlets crosscutting some of the pipe blocks (Fig. 3f). The pegmatite is melanocratic and is comprised primarily of clino- and orthopyroxenes, generally 0.5 to 1.0 cm in length but locally up to 3 cm in length. At the breccia pipe-host rock contact, the matrix pegmatite forms local apophyses up to about 10 cm in length into the host rock. The pegmatite also extends bilaterally from the pipe as dikes extending well into the surrounding, layered series rocks. One pegmatitic area located approximately 15 m west of the pipe is associated with a zone of brecciation 3×6 m, filled by fragments of wall rock (Ferguson and McCarthy 1970).

The region surrounding the pipe is characterized by local, crosscutting ultramafic veins. The contact of the

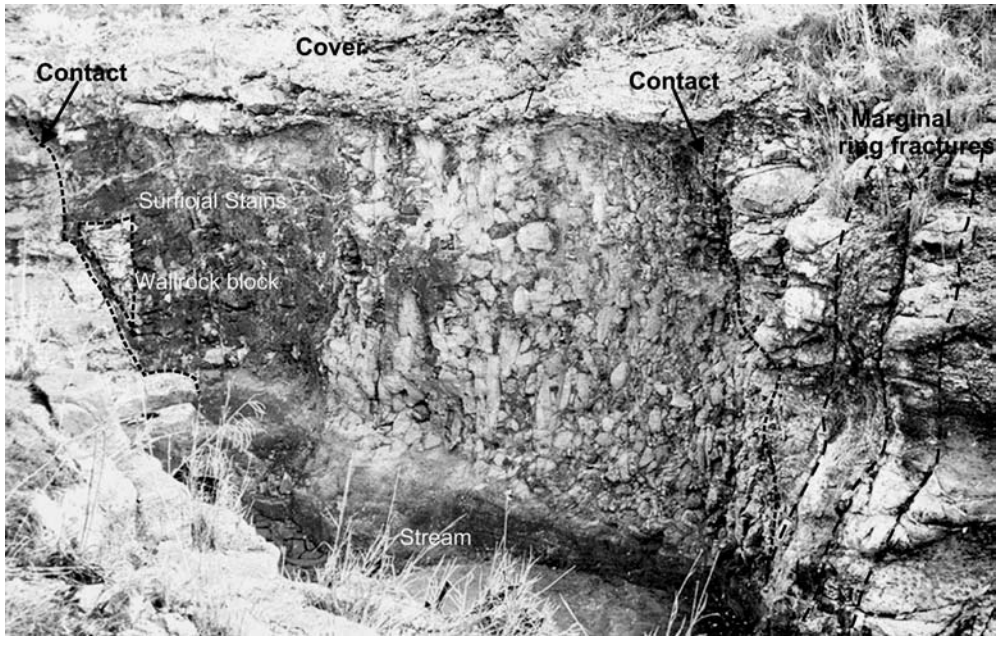

Fig. 2 Composite picture of breccia pipe exposure

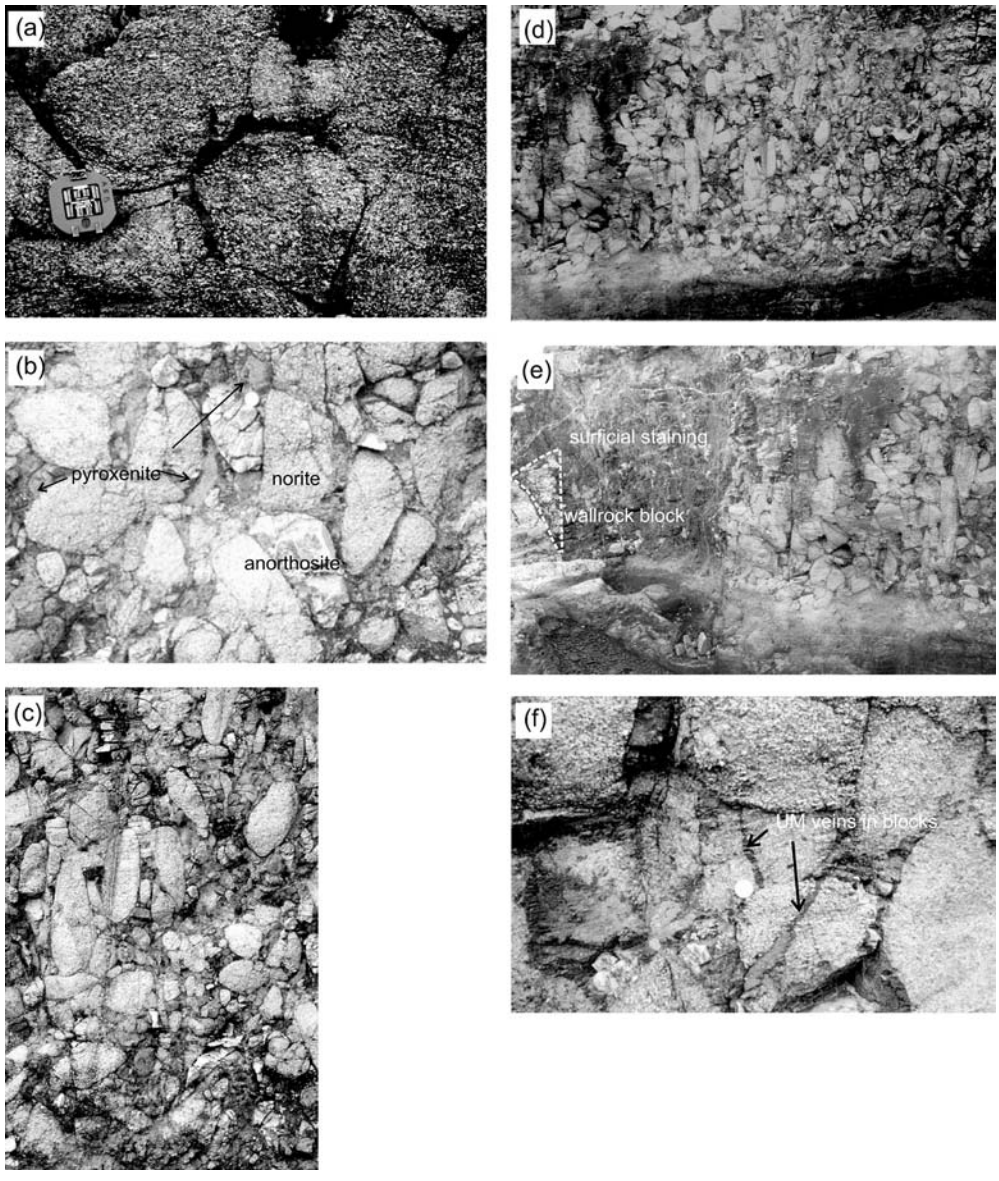

Fig. 3 **a** Blocks of Bushveld lithologies are fit tightly together in the body of the pipe. **b** A variety of Bushveld lithologies are entrained in the pipe. Norite anorthosite and pyroxenite blocks are labeled. **c** Elongate blocks are vertically oriented. **d** A size gradation is discernable between larger blocks in the center of the pipe (*left*) and smaller ones towards the edge of the pipe (*right*). **e** The western portion of the pipe has a darkish surficial staining (*left*). An angular piece of host rock has been entrained in the pipe (outlined in *dashed line*). **f** Blocks within the pipe are crosscut by ultramafic pegmatoidal veins

pipe contains small zones of brecciation wherein host rock forms angular fragments in a pegmatitic matrix. The breccia pipe is surrounded by a series of ring fractures in the host rock which are especially well exposed around the western side of the pipe where they are associated with ultramafic pegmatitic mineralization. These fractures are spaced at approximately 10-cm increments from the rim of the pipe to a distance of about 2–4 m from the pipe (Fig. 4). Such ring fractures have been described for other breccia pipe exposures (Calvari 2000).

The western portion of the exposure has previously been described as having been subject to intense amphibolitization, such that remnant outlines of blocks can

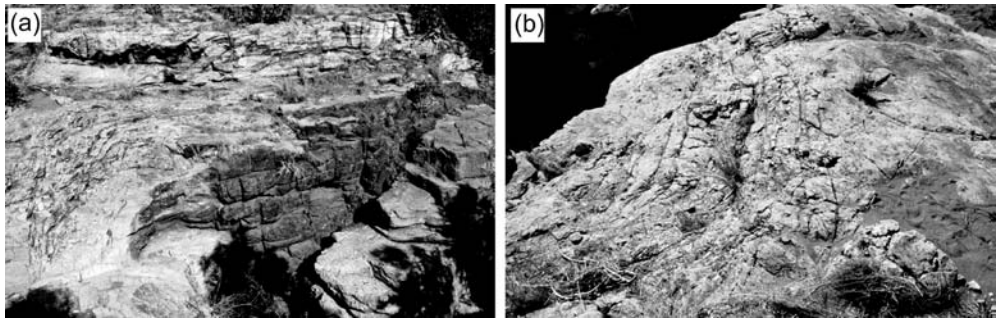

Fig. 4a, b Ring fractures around the perimeter of the breccia pipe. **a** North side of pipe (note ultramafic dike exposed). **b** South side of pipe

be discerned in some areas through a darker overprint (Ferguson and McCarthy 1970). In fact, this amphibolitization is locally surficial (Fig. 3e): when a surface is freshly exposed one can discern more features and the dark coloration appears to be a patina. In thin section, pyroxenes in these rocks are generally fresh, and have been only locally altered to amphibole along some grain edges.

Methods

Whole-rock composition data were collected from 18 breccia pipe blocks selected to cover the full compositional range of the pipe, as well as from four samples from the host rock adjacent to the pipe. Major-element abundances were determined by direct current plasma optical emission spectrometry (DCP-OES). Samples were prepared by the methods of Klein et al. (1991) on an ARL Fisons Spectroscan 7 DCP at Duke University. Trace-element abundances were obtained by VG-Elemental Quadrapole-3 inductively coupled plasma mass spectrometry (ICP-MS) at Duke University. Sample digestion and operating parameters are described in Meurer et al. (1999).

Mineral composition data for feldspars in breccia pipe blocks and in adjacent country rocks were collected by microprobe analysis at Duke University on a Cameca Camebax electron microprobe. Typical analysis conditions were 15-KeV acceleration voltage, 15-nA beam current, and 5–10 μm beam diameter. Peak and background counting times were 30 s on peak, and 15 s each on the high and low backgrounds.

Results

Major- and trace-element composition data are presented in Tables 1 and 2. Major-element geochemical data for breccia pipe norites, anorthosite, pegmatite groundmass and Critical Zone host rock are plotted on an AFS diagram, together with Bushveld compositional fields which are defined by ~120 samples from the Upper Critical Zone and Lower Main Zone (Scoon and Mitchell 1994; Fig. 5). Breccia pipe anorthosites plot within the anorthosite field. However, the breccia pipe norite compositions extend from the norite field, through the melanorite field towards more Fe-rich compositions. This range in noritic major-element composition may indicate a range in stratigraphic origin for the noritic blocks. Pegmatitic material analyzed from the breccia pipe falls into the Fe-poor end of the pegmatoid field defined on the plot.

In Fig. 6, anorthite content of feldspars from blocks within the pipe is compared to that of feldspar in the host rock, collected immediately adjacent to the pipe. Mean anorthite content for breccia pipe plagioclase is ~An_{83}, significantly higher than the mean anorthite content for country-rock feldspars (~An_{75}). Plagioclase in the breccia pipe rock was generally unzoned, as determined petrographically and by microprobe analysis. Anorthite content of breccia pipe feldspars is equivalent to that of feldspars in the Lower Critical Zone, about 800–1,000 m below the level of the breccia pipe. These results are compatible with the hypothesis that the

Table 1 Major-element data. *UM* Ultramafic, *anorth* anorthosite, *n.d.* not detected

Sample	2.2	2.3	2.4	2.5	3.1	3.2	4.2	4.3	4.4	4.5	4.6	4.7	4.8	4.9	4.10	4.11	4.12	4.14	4.15	4.16	4.17
Rock	Host	Host	Host	Host	Host	Host	UM	Norite	Anorth	Anorth	Norite	Norite	Anorth	Anorth	Norite	UM	Norite	Anorth	Anorth	Anorth	Anorth
SiO_2	52.24	49.5	49.5	49.9	49.5	52.3	52.6	48.1	49.3	48.9	52.8	49.8	48.2	47.4	47.8	52.6	51.1	48.6	45.0	49.4	45.0
TiO_2	0.36	0.08	0.11	0.14	0.10	0.40	0.44	0.27	0.09	0.08	0.39	0.13	0.07	0.07	0.08	0.43	0.39	0.11	0.11	0.12	0.11
Fe_2O_3	11.7	1.04	2.70	2.96	2.48	11.0	10.4	11.4	1.59	1.89	10.4	21.7	29.4	29.8	30.8	2.81	6.00	26.3	26.0	27.0	26.4
MnO	0.27	0.02	0.06	0.06	0.04	0.25	0.221	0.197	0.034	0.045	0.217	5.20	1.46	1.42	1.01	10.8	9.81	3.4	3.63	3.12	3.14
MgO	14.6	1.10	3.17	4.09	2.65	15.3	15.3	12.2	1.71	2.40	14.3	0.10	0.03	0.03	0.02	0.22	0.21	0.07	0.07	0.06	0.06
CaO	15.8	14.4	14.7	14.5	15.2	16.4	18.7	15.4	14.2	13.8	14.4	7.72	1.83	1.57	1.20	15.6	13.5	4.3	3.94	3.97	3.35
Na_2O	0.48	2.84	2.17	2.21	2.44	0.31	0.28	0.50	2.41	1.86	0.53	10.9	13.9	13.9	14.7	18.5	17.5	13.9	13.5	14.6	14.7
K_2O	0.0	0.03	0.60	0.37	0.18	0.12	0.09	0.48	0.86	1.38	0.23	1.97	1.60	1.49	2.31	0.32	0.49	2.05	2.30	1.95	2.21
Al_2O_3	6.94	30.4	27.2	27.0	27.8	4.37	2.63	11.4	29.2	28.7	6.13	0.09	1.76	1.77	0.76	0.06	0.09	0.14	0.13	0.18	0.35
P_2O_5	0.01	0.02	n.d.	0.28	0.01	0.03	0.02	0.01	0.02	0.02	0.04	0.01	0.01	0.02	0.02	0.01	0.01	0.01	0.02	0.02	0.01
LOI	0.15	–0.13	1.54	0.92	0.32	0.83	1.29	2.07	2.43	4.74	1.94	1.33	4.88	5.77	1.64	2.42	1.47	0.79	0.71	0.66	0.40
(%)																					
Total	102.2	99.4	100.2	101.1	100.4	100.4	100.5	99.5	98.5	97.6	99.1	97.5	96.4	95.7	98.6	101.3	99.0	98.8	99.6	100.4	100.3

Table 2 Whole-rock trace-element analyses (all in ppm by weight). *UM* Ultramafic, *n.a.* not analyzed

Sample	4.2	4.3	4.4	4.5	4.6	4.7	4.8	4.9	4.10	4.11	4.12	4.14	4.15	4.16	4.17	2.2	2.3	2.4	2.5	3.1	3.2
Rock	UM	Norite	Anorth	Anorth	Norite	Norite	Anorth	Anorth	Norite	UM	Norite	Anorth	Anorth	Anorth	Anorth	Host	Host	Host	Host	Host	Host
Ni	364	347	29	52	304	n.a.	35	32	n.a.	371	325	115	101	70	50	295	65	88	108	66	288
Zn	63	64	20	22	65	47	25	22	19	56	58	17	20	9	7	63	8	15	21	10	53
Co	81	87	20	19	73	47	16	15	21	73	72	30	28	20	15	75	21	28	31	21	68
Cu	15	5	8	8	6	9	8	8	9	6.7	6	15	13	7	8	8	13	12	13	10	7
Sr	27	433	5534	437	82	396	437	412	547	28	102	522	433	313	256	108	506	504	485	356	48
Sc	82	47.	6	6	68	14	8	6	3	82	70	11	9	6	6	62	4	9.0	11.4	6	73
Cr	1,010	502	79	174	1,004	738	263	155	40	1,388	1,040	273	161	187	101	623	43	173	302	110	617
Ba	14	206	250	294	48	100	476	515	289	17	27	110	97	59	68	47	122	260	173	90	10
V	553	308	42	35	422	72	47	35	415	511	463	75	59	500	67	57	28	n.a.	320	64	69
Zr	30	19	8	9	26	9	8	7	8	37	30	11	6	8	6	32	5	19	11	5	41
Y	21.8	12.3	3.2	3.3	23.8	4.8	4.1	3.3	9.2	24.3	19.3	6.1	5.1	25.8	6.3	3.5	2.2		28.0	4.6	9.7
Li	13	20	8	12	15	11	9	11	23	10	16	46	23	8	4	17	9	54	43	18	40
Be	0.79	0.82	4	3	2	2	4	4	5	1	0.89	1	0.87	0.69	0.73	0.51	0.81	1	1	1	1
Ga	6	10	20	19	9	16	21	21	22	5	7	18	17	12	10	9	20	19	20	15	8
Rb	1	17	23	56	6	9	86	82	22	1	2	4	3	2	3	1	3	14	9	1	1
Nb	0.49	0.34	0.54	0.60	1.29	0.32	0.51	0.46	0.46	0.91	0.59	0.40	0.32	0.33	0.21	0.54	0.11	0.49	0.88	0.17	0.81
Sb	1.59	2.85	3.96	2.28	3.17	0.80	4.09	2.81	2.63	1.40	1.88	1.22	0.57	0.17	0.69	0.81	0.22	1.76	1.27	0.19	0.90
Cs	0.15	0.35	0.73	1.24	0.25	0.33	2.17	1.96	0.86	0.12	0.20	0.42	0.26	0.23	0.31	0.15	0.16	0.67	0.59	0.08	0.07
La	3.21	2.61	5.86	5.48	6.44	3.53	6.02	5.95	6.59	3.75	3.26	6.27	4.08	3.20	2.54	3.02	3.08	6.58	8.12	2.89	5.41
Ce	11.9	7.48	10.5	9.85	20.63	6.73	10.8	10.6	10.9	13.9	11.3	11.3	7.67	6.92	4.76	9.88	5.37	12.20	17.26	5.22	17.52
Pr	6.84	3.87	3.43	3.39	10.64	2.30	3.84	3.62	3.45	7.89	6.34	1.29	0.88	0.87	0.59	1.65	0.62	1.42	2.12	0.63	2.76
Nd	10.8	6.10	3.70	3.70	15.33	2.73	4.33	4.03	3.69	12.36	9.94	5.11	3.25	3.42	2.12	8.93	2.20	6.02	9.92	2.34	15.07
Sm	3.43	1.97	0.69	0.68	4.08	0.57	0.82	0.74	0.67	3.78	3.01	0.99	0.69	0.74	0.46	2.68	0.39	1.20	2.13	0.44	3.84
Eu	0.55	0.63	1.19	1.13	0.62	0.63	1.34	1.30	1.19	0.52	0.57	0.95	0.70	0.57	0.44	0.41	0.59	0.91	0.96	0.46	0.60
Gd	3.60	2.09	0.60	0.61	4.10	0.51	0.81	0.73	0.55	4.16	3.26	0.97	0.69	0.66	0.45	1.54	0.49	1.05	1.54	0.45	2.22
Tb	0.60	0.33	0.08	0.08	0.65	0.08	0.11	0.09	0.07	0.70	0.54	0.16	0.10	0.11	0.07	0.52	0.06	0.18	0.34	0.07	0.73
Dy	3.70	2.17	0.46	0.51	3.98	0.50	0.62	0.53	0.40	4.20	3.30	0.78	0.50	0.59	0.34	3.16	0.20	0.99	1.80	0.35	4.39
Ho	0.74	0.43	0.09	0.10	0.82	0.11	0.12	0.10	0.08	0.86	0.68	0.16	0.10	0.11	0.07	0.63	0.04	0.20	0.36	0.07	0.86
Er	2.12	1.26	0.27	0.30	2.33	0.35	0.37	0.30	0.22	2.45	1.91	0.42	0.29	0.30	0.18	1.61	0.10	0.53	0.93	0.19	2.29
Yb	1.75	1.00	0.16	0.17	1.91	0.25	0.21	0.16	0.09	2.07	1.66	0.45	0.29	0.32	0.21	1.60	0.10	0.57	0.87	0.22	2.09
Lu	0.26	0.14	0.03	0.03	0.29	0.05	0.04	0.03	0.02	0.30	0.25	0.07	0.05	0.04	0.03	0.24	0.01	0.08	0.13	0.03	0.31
Hf	0.95	0.53	0.09	0.15	0.87	0.14	0.13	0.11	0.09	1.24	0.91	0.29	0.25	0.24	0.14	0.98	0.13	0.50	0.35	0.17	1.40
Ta	0.04	0.05	0.06	0.06	0.10	0.07	0.05	0.06	0.09	0.08	0.06	0.05	0.05	0.05	0.03	0.11	0.07	0.09	0.09	0.06	0.13
Pb	0.76	1.12	14.89	10.83	3.48	8.30	9.79	10.26	11.93	0.76	1.29	0.17	0.15	0.15	0.08	0.54	0.10	0.29	0.22	0.12	0.77
Th	0.27	0.13	0.29	0.18	0.76	0.09	0.25	0.16	0.27	0.27	0.18	0.22	0.20	0.09	0.08	0.28	0.04	0.24	0.22	0.05	0.27

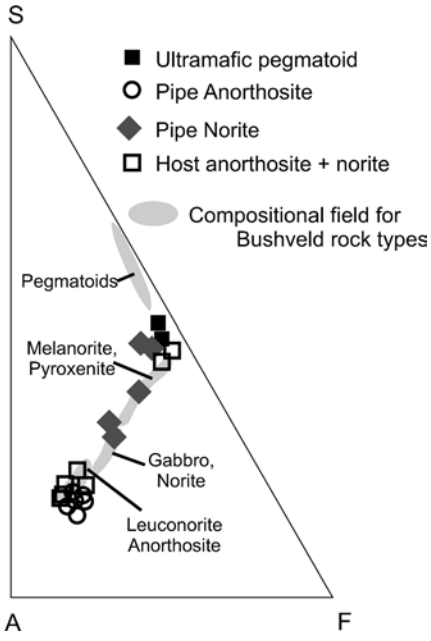

Fig. 5 Part of the ternary AFS plot where *A* is wt% ($Na_2O + K_2O + Al_2O_3$), *F* is wt% ($FeO + Fe_2O_3 + TiO_2 + CaO + MgO + MnO + P_2O_5$), and *S* is wt% SiO_2. Composition fields are for composite Upper Critical Zone/Main Zone lithologies (Scoon and Mitchell 1994)

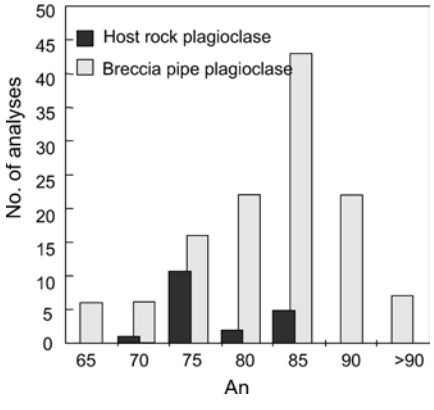

Fig. 6 Histogram of anorthite content. *Dark bars* are for host-rock plagioclase, *light bars* are for breccia pipe plagioclase

blocks within the breccia pipe underwent significant vertical transport.

Trace-element data from breccia pipe blocks were normalized to composite Critical Zone whole-rock compositions for each rock type (Willmore et al. 2000). Incompatible trace-element plots for anorthosites and norites are shown in Fig. 7. There is variation among norite samples (Fig. 7a), yet all are relatively depleted in P, and strongly enriched in the highly soluble element K. Norites are also generally enriched to varying degrees in the more soluble elements La, Ce, Ba, and Rb. Normative pyroxene is lower in the Willmore et al. (2000) norites than in the pipe norites, and thus breccia pipe norites appear relatively enriched in the elements which preferentially partition into pyroxene (e.g., Y).

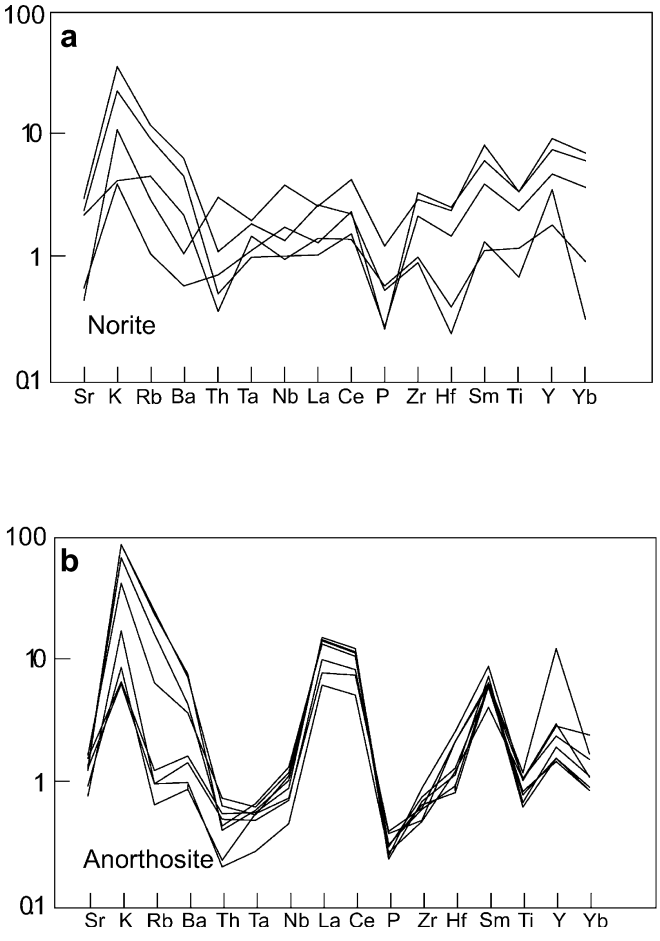

Fig. 7a, b Incompatible trace-element plots of whole-rock analyses of breccia pipe blocks normalized to composite Upper Critical Zone data for each lithology (Willmore et al. 2000). **a** Norites, and **b** anorthosites

The incompatible trace-element plot for anorthosites (Fig. 7b) shows similar general characteristics: a strong relative enrichment is observed in the soluble LILE and LREE elements K, La, Ce and Sm whereas the immobile elements Nb, Ta, Th, Hf and P are not enriched.

REE plots for breccia pipe anorthosites (Fig. 8a) show LREE enrichments and a positive Eu anomaly relative to in-situ Critical Zone anorthosite compositions. REE plots for the breccia pipe norites show dissimilarities in trace-element signatures, yet all samples show enrichment in aqueous fluid soluble elements relative to Critical Zone norites (e.g., alkalis and LREEs; Fig. 8b). The norite REE plot allows two groups to be distinguished: samples 4.10 and 4.7 are characterized by a negative Eu anomaly whereas samples 4.6, 4.11 and 4.12 have a positive Eu anomaly. This variation reflects the difference in bulk compositions in the norites, as seen on the AFS plot (Fig. 5): the samples whose compositions plot nearest the anorthosite field have a positive Eu anomaly, whereas those which plot in or near the norite field have a negative Eu anomaly, reflecting the variation in modal plagioclase.

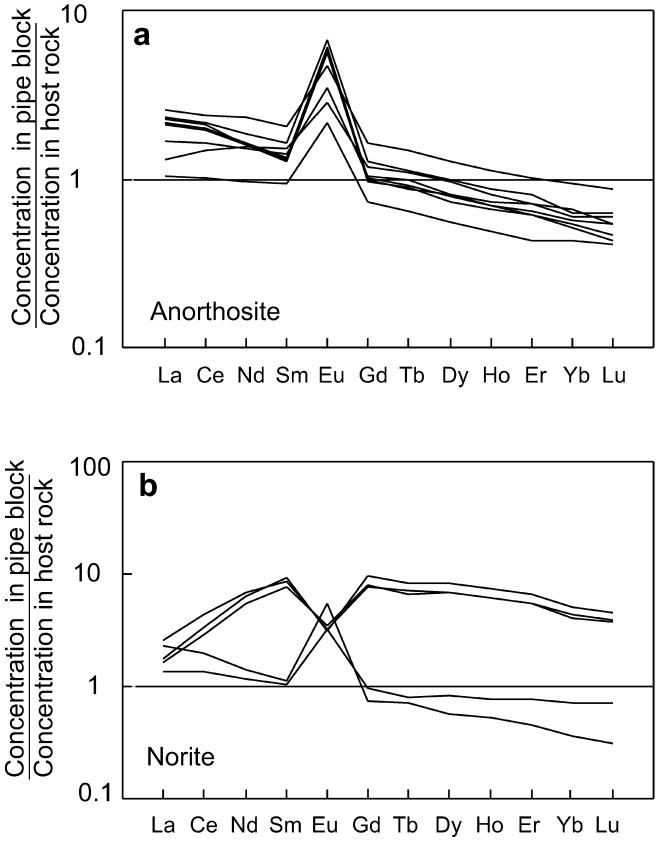

Fig. 8a, b Rare earth-element plots of whole-rock analyses of breccia pipe blocks normalized to composite Upper Critical Zone data for each lithology (Willmore et al. 2000). **a** Norites, and **b** anorthosites

Figure 9 shows the data for ultramafic pegmatites contained within the pipe, normalized to ultramafic pegmatoids from the Upper Critical Zone (Scoon and Mitchell 1994). Samples analyzed are in good agreement, with parallel patterns showing enrichment in the mobile elements K, Sr and Y relative to in-situ Critical Zone pegmatoids (Scoon and Mitchell 1994).

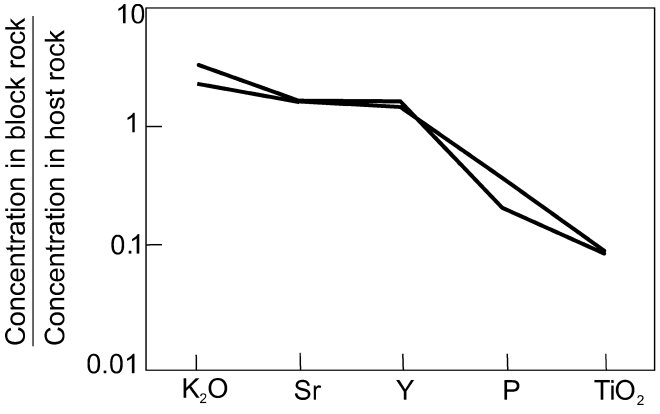

Fig. 9 Whole-rock data for Bushveld breccia pipe ultramafic pegmatoids normalized to Scoon and Mitchell (1994) Upper Critical Zone ultramafic pegmatoid composition data

Discussion

Evidence for volatile-induced fluidization of the blocks

Fluidization has commonly been invoked as an emplacement mechanism for kimberlite diatremes (e.g., Lorenz 1975; McCallum 1985), and in this paper we support the suggestion of Ferguson and McCarthy (1970) that the Bushveld breccia pipe may have been similarly emplaced. Fluidization can simply be viewed as an equilibrium state wherein the buoyant weight of a bed of particles is balanced by the upward drag force on the particles created by an upwardly moving fluid (Wilson 1984; Davidson et al. 1985). Fluidized bed technology has been extensively reviewed in the engineering literature, but little research has been conducted on fluidization in natural geologic processes. However, geologists have long observed clastic geologic materials behaving as a fluid (e.g., ignimbrites), and fluidization has become a common explanation for some geologic features. There are two lines of evidence which suggest the breccia pipe may have been emplaced by volatile-induced fluidization: observable physical features within and around the pipe, and geochemical features of the blocks from the pipe.

Physical evidence

If fluidization emplaced the blocks in the breccia pipe from elsewhere in the stratigraphy of the complex, one of several textural arrangements may be expected, depending on the velocity of the fluid and on characteristics of the blocks. For example, when fluidized particles move up a pipe-shaped container, the edges of the pipe retard the movement of the clasts nearest the edges of the pipe, causing particles in the center to have the greatest velocity (Davidson et al. 1985). This type of velocity gradient causes a size gradient in the pipe, with smaller blocks near the margins and larger blocks at the center (Davidson et al. 1985). Such a lateral size gradient is clearly preserved within the pipe (Fig. 3d; Ferguson and McCarthy 1970).

Blocks with high aspect ratios are generally oriented vertically, with their long axis perpendicular to the general stratigraphy of the complex and parallel to the long axis of the pipe (Fig. 3c), indicating vertical fluid movement. Seeing that the blocks maintain this orientation, one can infer that there was a significant solid fraction to the material which moved up the pipe during emplacement, such that the blocks did not significantly shift during cessation of fluid flow.

Geochemical evidence

If a volatile-rich igneous fluid was responsible for the emplacement of the Bushveld breccia pipe, then certain

geochemical signatures can be expected. For example, the enrichment of those incompatible elements soluble in igneous fluids (e.g., K, La, Ce, Sr, Ba) relative to immobile incompatible elements (e.g., P, Nb, Ta, Zr, Hf) has been interpreted as suggesting the presence of igneous fluids in pegmatoids in the Bushveld Complex (e.g., Boudreau et al. 1986; Cawthorn and Poulton 1988). By comparison, island-arc rocks are generally enriched in soluble elements (e.g., Ba, K, Sr, Sm), likely due to volatile-induced flux melting (Pearce 1983; Wilson 1984). Incompatible trace-element plots for norites and anorthosites show that the breccia pipe blocks are generally enriched in these and other soluble elements relative to similar host rocks, although norites show some intersample variation. Breccia pipe blocks (Fig. 7) are enriched in K, Rb, Sm, and Y. By contrast, a negative anomaly is observed for the immobile P, whereas the immobile elements Nb, Ti, Ta, Th, and Hf have values which nearly equal those of similar host cumulates. If these variations were due to variations in trapped liquid abundances, one would expect all incompatible elements, soluble and insoluble, to be enriched to a similar degree. Instead, these signatures are consistent with the blocks having been preferentially enriched in fluid-soluble incompatible elements from the transporting fluid.

REE plots of breccia pipe norites and anorthosites have a slight negative slope, showing some enrichment in LREEs relative to in-situ Bushveld rocks (Fig. 8). The variation among norite samples appears to reflect major-element chemistry: those samples which plot near the anorthosite field have a positive Eu anomaly, whereas those which plot near the melanorite field show a negative Eu anomaly. However, all the samples are strongly enriched in Nd, Y, Dy, and Er. The breccia pipe blocks have higher normative pyroxene than in-situ norites analyzed by Willmore et al. (2000). Though there is not conclusive evidence of fluid enrichment of soluble elements in the norites, our data are not inconsistent with such an interpretation.

Analysis of blocks of ultramafic pegmatite (Fig. 9) shows soluble-element enrichment, with K and Sr concentrations greater than twice those of in-situ pegmatites (Scoon and Mitchell 1994). The concentrations of immobile elements P and Ti are about equal to in-situ values. The breccia pipe pegmatites are also enriched in the immobile element Y.

The hypothesis that a volatile-rich phase formed the breccia pipe by violent degassing is supported by geochemical data obtained from the transported blocks within the pipe. Major-element data also lend validity to the hypothesis that the relative enrichment of soluble trace elements in the pipe anorthosites is due to mobilization of volatile-rich fluids. For example, Fig. 5 shows that there is little major-element compositional variation amongst the samples. This result is expected: bulk-rock major-element concentrations are buffered by modal mineralogy, and chemical variations due to exposure to a volatile-rich fluid phase are concentrated in the trace elements, and not in the major elements.

Furthermore, the more anorthitic plagioclase compositions of the blocks as compared to the host rock indicate that the blocks were not derived locally but were likely transported from below. It is possible that the plagioclase became more calcic during emplacement through late ionic exchange with a chlorine-rich fluid (e.g., Orville 1972):

However, optical examination and microprobe analysis of plagioclase show them not to be significant zoned. Hence, it seems unlikely that the plagioclase could have reached textural and compositional equilibrium with only a brief exposure to propellant fluid during a rapid pipe-forming event.

However, it is conceivable, and perhaps even likely, that the relatively higher An content of the pipe blocks is due to extensive ion exchange with fluid which took place between the plagioclase and a late fluid *prior to* the disruption event which formed the blocks. The expected long interval in which the fluid abundance and pressure was increasing in the source region would allow a longer equilibration time to produce unzoned, high-calcium plagioclase. In either scenario, most blocks were not derived from the immediate adjacent host, but were transported.

Mechanisms of breccia pipe formation

In the following discussion we consider the physical mechanisms for the formation of the Bushveld breccia pipe. We consider how overpressure can develop in vapor-saturated interstitial liquids as crystallization proceeds. We then find the minimum velocities the exsolved fluid would have to have achieved to lift the blocks seen in the breccia pipe. In the Appendix, a basic calculation demonstrates that the overpressure generated would be sufficient to generate these minimum velocities. Finally, we make a comparison between the Bushveld breccia pipe and kimberlite pipes, leading to a discussion of our proposed model for the emplacement of the Bushveld breccia pipe.

Development of overpressure from crystallization

Fluid overpressure can develop by a combination of two processes: (1) compaction of the crystal pile, such that any interstitial fluid supports a lithostatic load in excess of the hydrostatic pressure on the fluid, and (2) crystallization overpressure and fluid separating from an interstitial liquid which cannot escape from the crystal pile as fast as it is being generated. In the following we examine the second cause in more detail.

As anhydrous minerals crystallize from a vapor-saturated liquid, separation of a volatile-rich fluid must occur. This can lead to an overpressured situation. For example, Burnham (1979) has shown how differentiation-induced redistribution of water in a magma body can lead to local vapor saturation and to the rapid

upward migration of the vapor. Furthermore, the effect of degassing a fluid on magma pressures and on the eruption behavior of a shallow magma chamber has been examined by Tait et al. (1989). Boudreau (1992) broadened the discussion of the physical effects of the exsolution of a volatile phase by examining how degassing may cause overpressure in a solidifying crystal pile. In this study, we apply a crystallization model in order to determine how much overpressure is developed during the crystallization of a volatile, saturated interstitial liquid which crystallizes isochorically (constant volume).

We applied the PELE silicate-liquid crystallization model of Boudreau (1999), a PC-platform program based on the MELTS thermodynamic model of Ghiorso and Sack (1995). To approximate geochemical conditions of the crystallizing cumulate, Bushveld parental bulk compositions (Eales and Cawthorn 1996) were modified to represent the crystal-liquid assemblages which may have evolved in the crystal pile (Table 3). For example, to construct composition 1 a Critical Zone composition was allowed to crystallize in PELE until the first pyroxene crystallized. Composition 1 is then a 60:40 combination of the composition of the first pyroxene to crystallize and the liquid in equilibrium with these first crystals. Similarly, for composition 2, a bulk composition of 40% first pyroxene + 60% equilibrium liquid was used. Finally, for composition 3 a bulk composition of 60% first plagioclase + 40% equilibrium liquid was used. Crystallization of these bulk composition was modeled under both dry and water-saturated conditions.

In each of the dry runs, isochoric crystallization results in no overpressure above the starting pressure of 2,000 bar. In fact, pressure on the interstitial liquid drops dramatically. This decrease in pressure results from a net crystallization contraction in most crystallizing silicate phases – the solids take up less volume than the liquid (Peterson 1987). By contrast, in those isochoric runs where the crystallizing interstitial liquid is initially water saturated, significant overpressure can develop (Fig. 10). In all three cases, fluids were exsolved continually over the course of crystallization, but overpressure developed only when plagioclase joined the liquidus. This result is due to a relatively higher molar volume of plagioclase compared with that of the interstitial liquid. Thus, for overpressure to develop, the combined crystallization expansion of plagioclase and exsolution of water is required to overcome the crystallization contraction of the other crystallizing phases. Furthermore, the isochoric P–T plot of fluid-saturated magmas demonstrates that an overpressure of about 400 bar can be generated. Plagioclase-saturated liquids develop overpressures immediately, because plagioclase is the first mineral to crystallize, but less overpressure is developed.

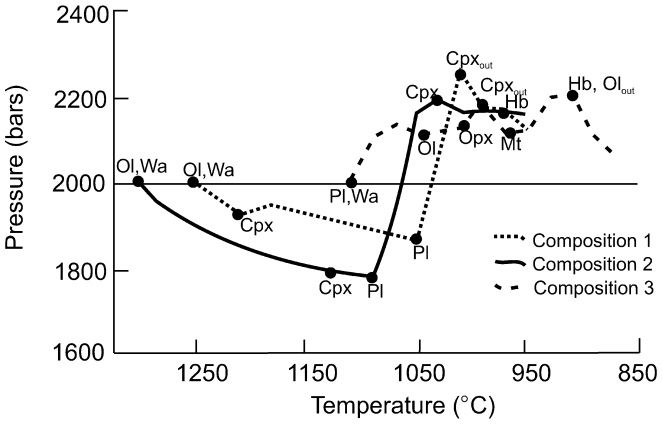

Fig. 10 Overpressure development during isochoric crystallization of three Bushveld magmas (Table 3). Incoming phases are labeled *Ol* olivine, *Pl* plagioclase, *Wa* water, *Cpx* clinopyroxene, *Opx* orthopyroxene, *Hb* hornblende, *Mt* magnetite. Outgoing phases are indicated by the *subscript out* (see text for discussion)

The requirement that plagioclase joins the liquidus for crystallization overpressure to develop is significant because the breccia pipe is located stratigraphically about 800 to 1,000 m above where plagioclase first appears as an abundant interstitial mineral: it is a modest but obvious increase in the amount of interstitial plagioclase which marks the base of the Lower Critical Zone.

Thus, the model results are consistent with our geochemical data: the plagioclase analyzed from pipe blocks has an average An content which does not disagree with an origin near the base of the Lower Critical Zone.

Table 3 Compositions used in fluid overpressure models

Number ID	1 Pyx60	2 Pyx40	3 Plag60
SiO_2	51.19	56.51	51.57
TiO_2	0.25	0.28	0.18
Al_2O_3	7.52	9.96	27.66
Fe_2O_3	1.35	1.20	0.44
FeO	4.67	7.39	1.68
MnO	12.66	0.05	0.06
MgO	17.21	15.22	1.15
CaO	0.98	5.64	12.27
Na_2O	0.47	1.48	2.72
K_2O	0.04	0.75	0.72
P_2O_5	0.04	0.07	0.07

Fluidization velocity

The fluidization velocity required to emplace the breccia pipe blocks can be determined by considering the minimum fluid velocity such that the upward drag force counteracts the gravitational force. Thus, to provide an estimate of minimum fluid ascent velocities, fluidization velocities are calculated using empirical equations for the turbulent suspension of non-spherical particles (Riba et al. 1978), such that fluidization velocity, v, is expressed as:

$$v=\frac{\mu}{d\rho_f}\left(\left(\left(\frac{12.0}{C_I}\right)^2+0.0114\left(\frac{d^3\rho_f^2 g}{\mu^2}\right)\left(\frac{Mv}{\psi^{3.2}C_I}\right)\right)-\frac{12.0}{C_I}\right)$$

where d is the diameter of the particle, μ is the viscosity of the fluid, and ρ_f is the density of the fluid. C_I represents the inertial drag coefficient. For fluids with a sphericity factor (ψ) less than 0.8 (Howard 1989), C_I is approximated by $2.53-2.83e^{2.3\psi}$. This C_I value assumes a Reynold's number of between 200 and 500, a low-end assumption for our scenario. Finally, Mv is the density ratio, and is equal to $\frac{\rho_b-\rho_f}{\rho_f}$ where ρ_b is the density of the block. The density of the volatiles will be assumed to be that of water (1,000 kg/m^3), and the density of the blocks is assumed to be 2,700 kg/m^3. The assumption that the density of the fluids is that of water forms the low end-member scenario. Of course, the fluid here will not be pure water and will probably be significantly denser than water due to dissolved species carried in it. The effects of fluid densities ranging from that of water to 2,500 kg/m^3 are considered in more detail in Fig. 11. The acceleration due to gravity (g) is 9.81 m/s^2, and the viscosity of the liquid is taken to be that of water, 0.01 Pas. Although these equations were derived for small (micron scale) particles, the values obtained have generally been deemed acceptable for much larger geologic materials (e.g., Wilson 1984; McCallum 1985).

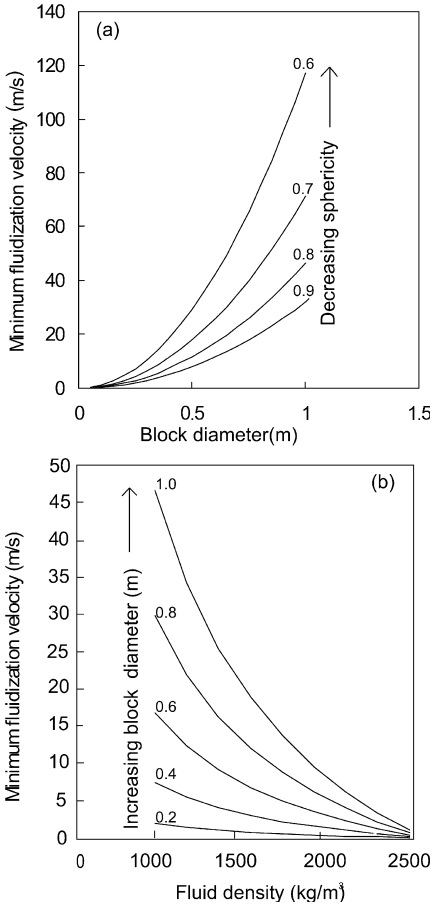

Fig. 11a, b Results from minimum fluidization calculations (see text for discussion). **a** Block diameter, and **b** fluid density relationships

The results of the velocity calculations are shown in Fig. 11, where minimum fluidization velocity is plotted for various conditions. Block diameter is plotted against velocity for different shape factors (Fig. 11a), showing an expected result of greater diameters and greater sphericity requiring greater emplacement velocities. It is useful to consider ascent velocities for particles with different fluid densities (Fig. 11b) to account for dissolved species increasing the density of the exsolved phase. As fluid density increases, the minimum fluidization velocity required to emplace the blocks decreases. Ascent velocity must be greater than the minimum fluidization velocity, so the values shown in the figure define the lower boundary of velocity conditions. Maximum velocity is unconstrained, but Fink and Kieffer (1993) calculate a maximum expansion rate of 170 m/s for pyroclastic eruptions. Our values seem to be in line with these estimates, with the most spherical blocks (shape factor = 0.9) having minimum fluidization velocities reaching about 120 m/s.

The controlling factors in calculating the conditions which existed during formation of the Bushveld breccia pipe seem to be the shape of the ascending blocks, and the nature and composition of the ascending liquid. If the volatile fluid included significant dissolved material, then both the viscosity and density of the resultant liquid would increase, giving more transport ability and decreasing the required minimum velocity. The most realistic minimum ascent velocities are obtained for an ascending liquid which was mostly volatile with some dissolved ultramafic melt component, allowing the degassing crystal pile to move blocks through a spouting flow. However, the calculations do not take into account the complications of having more than one type of block being fluidized. Our calculations do not allow for variations in xenolith density, and the irregularity of their shape may not be well expressed by sphericity factors. Calculations presented in the Appendix show that crystallization overpressure can generate the minimum fluidization velocities calculated here.

Kimberlite comparison

The Bushveld breccia pipe can be compared to kimberlite pipes based on their physical form, geochemical characteristics, the role of fluid overpressure, and emplacement mechanisms. Kimberlite bodies are pipe-shaped with steep (~80–84°), sharp contacts with the surrounding country rocks (Novikov and Slobodskoy 1978). Kimberlite pipes often occur within a network of fractures, and are generally associated with linear dikes (Kurslauskis et al. 1998). Kimberlite pipe xenoliths are transported from below or above, such that blocks transported from below tend to be rounded whereas those falling from above tend to be angular (Novikov and Slobodskoy 1978). Kimberlite xenoliths are commonly flattened, with a predominant long axis between 0.3 and 0.7 m long (Novikov and Slobodskoy 1978;

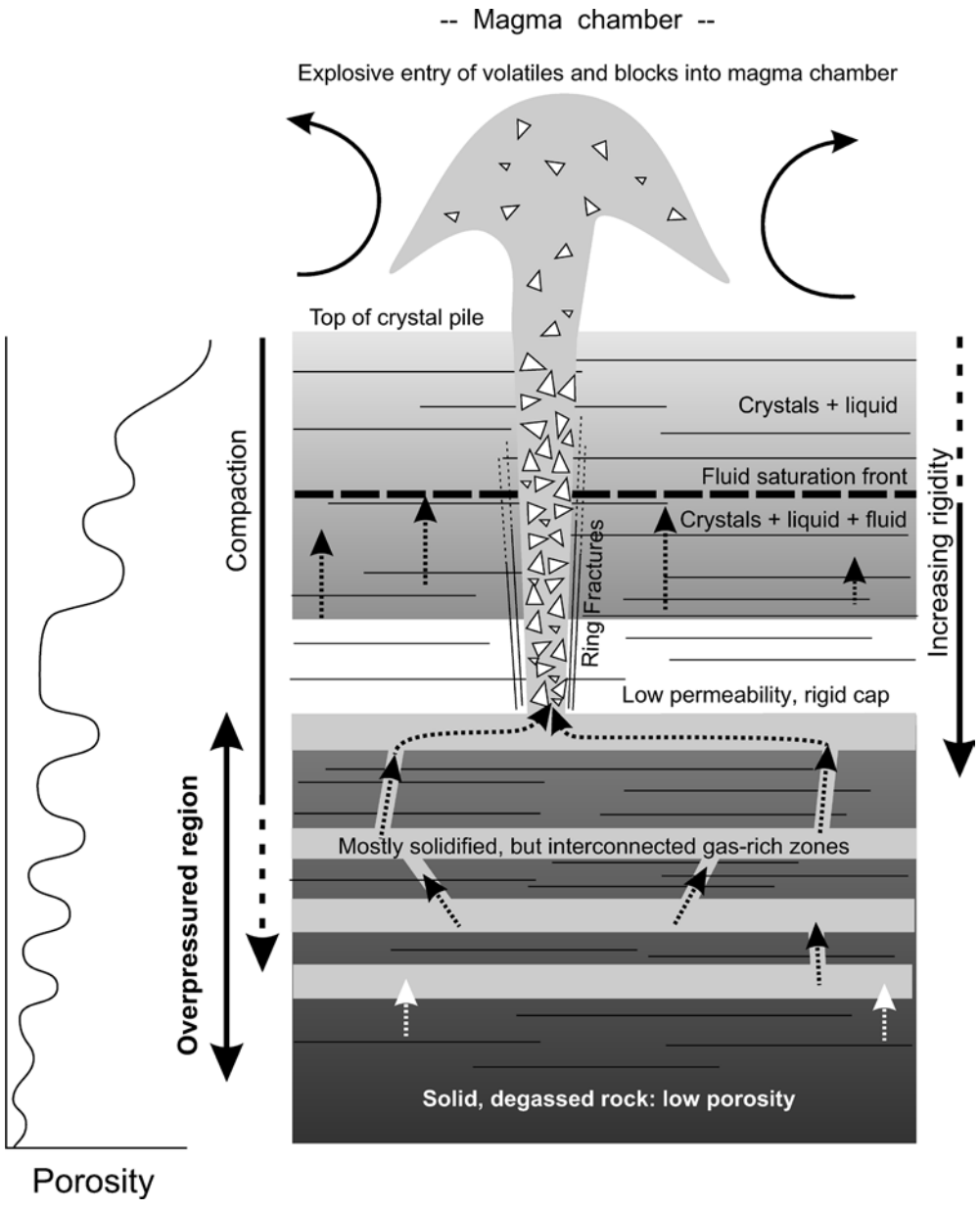

Fig. 12 Schematic illustration of overpressure development and pipe emplacement. The base of the chamber is solid degassed cumulates, with no porosity. This region is overlain by a region of crystal mush, wherein exsolving fluids migrate upwards along a pressure gradient to a fluid saturation front within the mush zone (crystals and liquid). Overpressure develops beneath the fluid saturation front, leading to the explosive emplacement of the breccia pipe, and the possible release of volatiles back into the main magma chamber

Kurslauskis et al. 1998). Locally derived xenoliths are concentrated around the periphery of the pipe whereas those transported from below tend to be concentrated preferentially in the center of the kimberlite pipe (e.g., Novikov and Slobodskoy 1978). Kimberlites also may be surrounded by breccias of the country rocks in the exocontact where the matrix is comprised of the kimberlite pipe matrix (Novikov and Slobodskoy 1978).

The Bushveld breccia pipe has similar features. It is characterized by a vertical pipe-like body, emplaced along a linear set of ultramafic dikes, and in a network of fractures. Breccia pipe blocks are arranged in a way similar to kimberlite pipes: angular host-rock fragments are at the edge of the pipe whereas rounded, commonly elongate blocks are in the center. The periphery of the pipe is comprised of an angular breccia, where the matrix appears to be the same, pegmatitic matrix filling in the interstices of the breccia pipe, similar to exocontact regions in kimberlite pipes.

There is a vigorous debate regarding whether kimberlite pipes are emplaced via a fluidization mechanism resulting from exsolving CO_2 and H_2O or from a phreatomagmatic process(e.g., Kurslauskis et al. 1998; Beard et al. 1999). Velocities for the phreatomagmatic emplacement of breccia pipes have been experimentally determined to be between 200 and 400 m/s (Zimanowski et al. 1991; Kurslauskis et al. 1998). A fluidization model discussed by Novikov and Slobodskoy (1978) gives emplacement velocities of about 100–200 m/s. These models agree with our minimum fluidization velocities calculated for emplacement of the blocks in the Bushveld breccia pipe.

A comparison between kimberlite pipe and Bushveld breccia pipe trace-element geochemistry shows that,

although both are enriched in soluble elements, kimberlite pipes are generally enriched to a much greater degree (e.g., Beard et al. 1999; O'Brien and Tyni 1999). However, spidergrams for both have a negative slope, and pronounced positive Ba and negative P anomalies (O'Brien and Tyni 1999).

Thus, a comparison between physical characteristics of kimberlite pipes and the Bushveld breccia pipe holds up quite well. The trace-element geochemistry has some similarities, but differences can be explained by the different sources for each, and therefore we present a model for the emplacement of the Bushveld breccia pipe based on the fluidization model for kimberlite emplacement. We envision a scenario which is illustrated in Fig. 12 for the explosive emplacement of the breccia pipe due to overpressure from exsolved fluids. Fluid saturation in the interstitial liquid of the crystal pile occurs after volatile concentrations are increased in the liquid as the result of the crystallization of anhydrous phases. The net volume change on crystallization is usually negative (Peterson 1987), leading to a net contraction but, when fluids are exsolved and plagioclase crystallizes, the net volume change is positive and a crystallization overpressure develops. This overpressure is in addition to any overpressure from derived compaction in the crystallizing pile. Thus, as seen in Fig. 12, the base of the chamber comprises solid degassed cumulates, with no porosity. This region is overlain by a region of crystal mush, wherein exsolving fluids migrate upwards along a pressure gradient to a fluid saturation front within the mush zone (crystals and liquid). Overpressure develops beneath the fluid-saturation front, leading to the eventual explosive emplacement of the breccia pipe and the possible release of volatile components back into the main magma chamber.

Because the Lower and Critical zones are characterized by modal layering, it is likely that different bulk-rock compositions will have different solidus temperatures – some lithologies will be more permeable to fluid transport than others. Fluids are likely to collect in those rocks which have significant residual porosity. These gas-rich regions may be interconnected via pegmatitic channel ways and fractures. Conversely, rocks with low permeability can act as "caps" preventing the escape of fluids. When an escape channel does develop, the fluid escapes violently. The presence of ring fractures suggests the exposed host rock (as with the blocks themselves) was significantly solidified such that the fracturing was not annealed subsequent to pipe formation. This suggests that the fluid-source region was gas-rich and silicate-liquid poor.

Conclusions

This study supports earlier contentions that exsolved fluids can create significant overpressures in a solidifying crystal pile (Burnham 1979; Boudreau 1992). Furthermore, we add to the growing body of work supporting the importance of exsolved fluids migrating upwards as they harvest and concentrate any PGE which may be present in layered intrusions. Thus, we reiterate the ideas of volatile-induced PGE enrichment supported in Stumpfl's work. In fact, we propose that, given the Cl nature of these propellant fluids (e.g., Willmore et al. 2000), late reaction of this fluid with host rock can result in an iron-rich solution. Indeed, the overpressured gas may effectively "steam clean" host rock of pyroxene when allowed to fully react with hotter rock as it migrates through the crystal pile. The ultramafic material found between the blocks in the pipe, and found in pegmatites and veins surrounding the pipe and elsewhere in the Bushveld complex, is reasonably inferred to be late precipitates from this Fe-rich fluid.

Acknowledgements It is a pleasure to contribute to this volume in honor of Eugen Stumpfl, in recognition of his lifelong work in the Bushveld Complex. We thank C. Ballhaus and E. Mathez for their constructive reviews of this paper. Part of this work was a senior thesis by JBM. This work was supported by US National Science Foundation Grant 99-02183.

Appendix

Darcy's law can be used to translate pressure differentials into fluid velocities. If we take the crystallization overpressure to be 400 bar (Fig. 10), the overpressure can be expressed in terms of change in head in an aquifer,

$$dh = dP/\rho_r g$$

where dP = crystallization overpressure (400 bar = 400×10^7 N/m^2), dh = change in head (m), g = acceleration due to gravity, ρ_f = density of the fluid (water), and then the Darcy velocity can be calculated as:

$$v_d = \left(Cd^3\gamma/\mu\right)(dh/dl)$$

where v_d = Darcy velocity (discharge/area), C = shape factor, d = pore diameter, γ = specific gravity, μ = viscosity, dh = change in head, and dl = pipe length.

The shape factor, C, is related to the sphericity of the particles, and has values ranging from about 10 to 150.We choose a value of 100 for our calculations, but velocity calculations are not very sensitive to particle shape. The velocity is proportional to pore diameter (d) cubed for ideal pipe flow. The specific gravity, γ, is found as $g\rho$, where ρ is the density of the particles (blocks). The viscosity of water is used to approximate fluid viscosities. The term dh/dl is a measure of how pressure decreases along the length of the pipe (dh is calculated from dP; see above). The length of the pipe, dl, is estimated to be between 800 and 1,000 m.

These calculations show that an overpressure of 400 bar generates more than sufficient velocities to explosively emplace the breccia pipe >800 m in length. The velocities generated are on the order of 1,000 m/s, higher than most but not all estimated kimberlite emplacement velocities (Artyushkov and Sobolev 1984).

References

Artyushvkov EV, Sobolev SV (1984) Physics of kimberlite magmatism. In: Kornprobst J (ed) Kimberlites I: kimberlites and related rocks. Proc 3rd Int Kimberlite Conf, vol 1. Elsevier, Amsterdam, pp 309–322

Ballhaus CG (1988) Potholes of the Merensky reef at the Brakspruit shaft, Rustenburg platinum mines; primary disturbances in the magmatic stratigraphy. Econ Geol 83:1140–1158

Ballhaus CG, Stumpfl EF (1985) Occurrence and petrological significance of graphite in the Upper Critical Zone, western Bushveld Complex, South Africa. EPSL 74:58–68

Beard A, Downes H, Hegner E, Sablukov S, Vetrin V, Balogh K (1999) Mineralogy and geochemistry of Devonian ultramafic minor intrusions of the southern Kola Peninsula, Russia: implications for the petrogenesis of kimberlites and melitites. Contrib Mineral Petrol 130:288–303

Boudreau AE (1992) Volatile fluid overpressure in layered intrusions and the formation of potholes. Aust J Earth Sci 39:277–287

Boudreau AE (1999) PELE – a version of the MELTS software program for the PC platform. Comput Geosci 25:201–203

Boudreau AE, Kruger FJ (1990) Variation in the composition of apatite through the Merensky cyclic unit in the western Bushveld Complex. Econ Geol 85:737–745

Boudreau AE, McCallum S (1989) Investigation of the Stillwater Complex. Part V. Apatites as indicators of evolving fluid composition. Contrib Mineral Petrol 102:138–153

Boudreau AE, Mathez EA, McCallum IS (1986) Halogen geochemistry of the Stillwater and Bushveld complexes: evidence for the transport of the platinum group elements by Cl-rich fluids. J Petrol 27:967–986

Buntin TJ, Grandstaff DE, Ulmer GC, Gold DP (1985) A pilot study of geochemical and redox relationships between potholes and adjacent normal Merensky Reef of the Bushveld Complex. Econ Geol 80:975–987

Burnham CW (1979) Magmas and hydrothermal fluids. In: Barnes HL (ed) Geochemistry of hydrothermal ore deposits, 2nd edn. Wiley, New York, pp 71–136

Calvari S (2000) Stages in Sortino diatreme formation, eastern Sicily, Italy. AGU Abstr Programs, Fall Meet 2000

Cawthorn RG, Poulton KL (1988) Evidence for fluid in the footwall beneath potholes in the Merensky Reef of the Bushveld Complex. In: Prichard HM, Potts PJ, Bowles JFW, Cribbs SJ (eds) Geoplatinum 87. Elsevier, Amsterdam, pp 343–356

Davidson JF, Clift R, Harrison D (1985) Fluidization. Academic Press, London

Eales, Cawthorn RG (1996) The Bushveld Complex. In: Cawthorn RG (ed) Layered intrusions. Elsevier, Amsterdam, pp 181–229

Ferguson J, McCarthy TS (1970) Origin of an ultramafic pegmatoid in the eastern part of the Bushveld Complex. Geol Soc S Afr Spec Publ 1:74–79

Fink JH, Kieffer SW(1993) Estimate of pyroclastic flow velocities resulting from explosive decompression of lava domes. Nature 363:612–615

Ghiorso MS, Sack RO (1995) Chemical mass transfer in magmatic processes. IV. A revised and internally consistent thermodynamic model for the interpolation and extrapolation of liquid-solid equilibria in magmatic systems at elevated temperatures and pressures. Contrib Mineral Petrol 119:197–212

Howard JR (1989) Fluidized bed technology: principles and applications. A Hilger, Bristol

Klein EM, Langmuir CH, Staudigel H (1991) Geochemistry of basalts from the southeast Indian Ridge, 115 E–138 E. J Geophys Res 96:2089–2107

Kruger FJ (1994) The Sr-isotopic stratigraphy of the western Bushveld Complex. S Afr J Geol 97:393–398

Kruger FJ, Marsh JS (1982) Significance of $^{87}Sr/^{86}Sr$ ratios in the Merensky cyclic unit of the Bushveld Complex. Nature 298:53–55

Kruger FJ, Cawthorn RG, Meyer PS, Walsh KL (1986) Sr-isotopic, chemical and mineralogical variations across the pyroxenite marker of the Upper Zone of the western Bushveld Complex. In: Proc Geo-Congress 1986, Johannesburg. Geol Soc S Afr, pp 609–612

Kurszlaukis S, Buttner R, Zimanowski B, Lorenz V (1998) On the first experimental phreatomagmatic explosion of a kimberlite melt. J Volcanol Geotherm Res 80:323–326

Lorenz V(1975) Formation of phreatomagmatic maar-diatreme volcanoes and its relevance to kimberlite diatremes. In: Proc 1st Int Conf Kimberlites. Phys Chem Earth9:17–27

McBirney AR, Naslund HR(1990) The differentiation of the Skaergaard Intrusion. Contrib Mineral Petrol 104:235–240

McBirney AR, Sonnenthal EL(1990) Metasomatic replacement in the Skaergaard Intrusion, East Greenland; preliminary observations. Chem Geol 88:245–260

McCallum ME (1985) Experimental evidence for fluidization processes in breccia pipe formation. Econ Geol 80:1523–1543

Meurer WP, Willmore CC, Boudreau AE (1999) Metal redistributing during fluid exsolution and migration in the Middle Banded Series of the Stillwater Complex, Montana. Lithos 47:143–156

Mogessie A, Stumpfl EF, Weiblen PW (1991) The role of fluids in the formation of platinum group minerals, Duluth complex, Minnesota: mineralogic, textural and chemical evidence. Econ Geol 86:1506–1518

Nicholson D, Mathez E (1991) Petrogenesis of the Merensky reef in the Rustenburg section of the Bushveld Complex. Contrib Mineral Petrol 107:293–309

Novikov L, Slobodskoy R (1978) Mechanism of formation of diatremes. Int Geol Rev 21:1131–1139

O'Brien H, Tyni M (1999) Mineralogy and geochemistry of kimberlites and related rocks from Finland. In: Proc 7th Int Kimberlite Conf, pp 625–636

Orville PM (1972). Plagioclase cation exchange equilibria with aqueous chloride solution: results at 700 °C and 2000 bars in the presence of quartz. Am J Sci 272:234–272

Pearce JA (1983) The role of sub-continental lithosphere in magma genesis at destructive plate margins. In: Hawkesworth CJ, Norry MJ (eds) Continental basalts and mantle xenoliths. Nantwich, Shiva, pp 230–249

Peterson JS (1987) Solidification contraction: Another approach to cumulus processes and the origin of igneous layering. In Parsons I (ed) Origins of igneous layering. D Reidel, Boston, pp 505–526

Riba JP, Routie R, Couderc JP (1978) Minimal conditions for fluidization by a liquid. Can J Chem Eng 56(1):26–30

Scoon R, Mitchell A (1994) Discordant iron-rich ultramafic pegmatites and their relationship to iron-rich intercumulus and residual liquids. J Petrol 35:881–917

Stumpfl EF, Rucklidge JC (1982) The platiniferous dunite pipes of the eastern Bushveld Complex. Econ Geol 77:1419–1431

Stumpfl EF, Tarkian M (1976) Platinum genesis: new mineralogical evidence. Econ Geol 71:1451–1460

Tait S, Jaupert C (1992) compositional convection in a reactive crystalline mush and melt differentiation. J Geophys Res 97:6735–6756

Tait S, Jaupert C, Vergniolle S (1989) Pressure, gas content and eruption periodicity of a shallow, crystallizing magma chamber. EPSL 92:107–123

Viljoen MJ, Scoon RN (1985) The distribution and main geologic features of discordant bodies of iron-rich ultramafic pegmatite in the Bushveld Complex. Econ Geol 80:1109–1128

Walraven F (1988) Notes on the age and genetic relationships of the Makhutso granite, Bushveld Complex, South Africa. Chem Geol 72:17–28

Willmore CC, Boudreau AE, Kruger FJ (2000) The halogen geochemistry of the Bushveld Complex, Republic of South Africa: Implications for chalcophile element distribution in the Lower and Critical zones. J Petrol 41:1517–1539

Wilson CJN (1984) The role of fluidization in the emplacement of pyroclastic flows. 2. Experimental results and their interpretation. J Volcanol Geotherm Res 20:55–84

Zimanowski B, Frohlich G, Lorenz V (1991) Quantitative experiments on phreatomagmatic explosions J Volcanol Geotherm Res 48:341–358